The energy and water dynamics of a central Amazonian rain forest

Y. Malhi,[1] E. Pegoraro,[1] A. D. Nobre,[2] M. G. P. Pereira,[3] J. Grace,[1] A. D. Culf,[4] and R. Clement[1]

Received 12 March 2001; revised 22 October 2001; accepted 20 November 2001; published XX Month 2002.

[1] This paper presents measurements of the energy and water budgets of a tropical rain forest near Manaus, Brazil, in central Amazonia, collected between September 1995 and August 1996. Fluxes of sensible and latent heat were measured using a three-dimensional eddy covariance system mounted above the forest canopy. Using a new approach to analysis of eddy covariance data, we found that the measured fluxes increased significantly when turbulent transport on timescales of 1 to 4 hours was taken into account. With this new analysis, the measured turbulent fluxes almost perfectly balanced the incoming net radiation, giving increased confidence in the accuracy of the measured fluxes. Of the 5.56 GJ m^{-2} yr^{-1} of solar radiation supplied over the year, 11% were reflected, 15% were lost as net thermal emission, 27% were transported through sensible heat convection, 46% used in evapotranspiration, and 0.5% were used in net carbon fixation. Total annual evapotranspiration was calculated to be 1123 mm, accounting for 54% of total precipitation. Seasonality was an important influence: limited water availability during the dry season caused evapotranspiration to reduce by 50%. Total canopy conductance was linearly correlated to soil moisture content, with typical midday values ranging between 0.8 mol m^{-2} s^{-1} in the wet season and 0.3 mol m^{-2} s^{-1} in the dry season. Such seasonal behavior is likely to be prevalent in most tropical forest regions, and correction description of dry-season evapotranspiration will require accurate modeling of plant and soil hydraulic properties and knowledge of root distributions. *INDEX TERMS:* 1878 Hydrology: Water/energy interactions; 3322 Meteorology and Atmospheric Dynamics: Land/atmosphere interactions; 1655 Global Change: Water cycles (1836); 1818 Hydrology: Evapotranspiration; 1812 Hydrology: Drought; *KEYWORDS:* Energy balance, water balance, tropical forest, soil moisture, eddy covariance, eddy correlation, forest, evapotranspiration, Amazon, flux, carbon dioxide

1. Introduction

[2] Tropical rain forests are characterized by a water-rich environment. They girdle the Earth's terrestrial equatorial regions, covering 17.6 million km^2 (FAO 1993), 13% of total land surface area (excluding Antarctica). Amazonia hosts the largest block of tropical rain forest, about 50% of the total [*Malhi and Grace*, 2000]. They generate a major part of global land surface evaporation [*Choudhury et al.*, 1998], thereby exerting a significant influence on the global hydrological cycle. In turn, this intense evaporation drives tropical convection, and has a major influence on the global atmospheric circulation.

[3] Understanding of the controls of the seasonal variation of these fluxes in the terrestrial tropics is still poor, and depends crucially on how tropical vegetation uses energy and water. Important issues included the extent to which tropical forests recycling water vapour back into the atmosphere (25–35% of rain that falls in the Amazon basin is contributed by evaporation within the basin: [*Eltahir and Bras*, 1994; *Trenberth*, 1999]), and the extent to which they can continue transpiring in the dry season or during El Niño-associated droughts [*Nepstad et al.*, 1994]. There is also a threat that the nature of these exchanges is changing at a globally significant extent, as deforestation continues unabated [*Laurance et al.*, 2001]. Global climate model simulations suggest that large-scale deforestation of Amazonia would lead to a regional surface temperature increase between 0 and 2°C, and reductions of evaporation and precipitation of about 25%. These reductions would in turn cause further negative impacts on forest function and transpiration [*Nobre et al.*, 1991; *Henderson-Sellers*, 1993; *Dirmeyer and Shukla*, 1994; *Xue et al.*, 1996].

[4] However, there exist only a few field studies of the exchange of water between rain forests and the atmosphere [e.g., *Shuttleworth et al.*, 1984; *Shuttleworth*, 1989; *Roberts et al.*, 1993; *Grace et al.*, 1995]. Early studies either used traditional micrometeorological techniques or else one-dimensional correlation techniques. While representing a significant advance in flux measurement techniques, one-dimensional eddy covariance measurements were prone to

[1]Institute of Ecology and Resource Management, University of Edinburgh, Edinburgh, Scotland, UK.
[2]Instituto Nacional de Pesquisas da Amazônia, Manaus, Amazonas, Brazil.
[3]Universidade Federal de Viçosa, Minas Gerais, Brazil.
[4]Centre for Ecology and Hydrology, Wallingford, UK.

0148-0227/02/2001JD000623$09.00

errors associated with advection and nonperfect leveling of the instrumentation, and have largely been abandoned on favor of three-dimensional eddy covariance techniques. *Grace et al.* [1995] used three-dimensional eddy covariance to collect 55 days of measurements from a forest in Rondonia, southern Amazonia.

[5] Here we report results from the first long-term measurements of heat and water fluxes over a tropical forest using full three-dimensional sonic anemometry. We present results from a year of measurements from a primary rain forest in central Amazonia in 1995–6. The carbon dioxide fluxes above this forest have been described by *Malhi et al.* [1998], and a model-based exploration of the physiological constraints on photosynthesis was presented by *Williams et al.* [1998].

2. Site

[6] The experimental site was located some 60 km north of Manaus, Amazonas, Brazil, in the Reserva Biológica do Cuieiras (2°35′22″S, 60°06′55″W), a forest reserve belonging to the Instituto National de Pesquisas da Amazônia (INPA). The site is situated on a very extensive plateau (90 m above sea level) dissected by occasional broad river valleys, with a dense lowland *terra firme* tropical rain forest characterized by a canopy height of 30m, an aboveground dry biomass of 300–350 t ha^{-1} and a very high leaf area index which ranges between about 5 in the dry season and 6 in the wet season. This site is typical of the natural vegetation and topography of much of central Amazonia.

[7] The plateau soil is a yellow clay latosol (Brazilian classification) or oxisol (U.S. Department of Agriculture soil taxonomy), with a high clay content (80%), low nutrient content and a low pH (4.3). Much of the porosity is concentrated in the macropores and large mesopores [*Chauvel et al.*, 1991], through which water drains rapidly, and in very fine pores, which contains water not accessible to plants. This results in a very low available water capacity, 70 mm m^{-1} in the upper meter of the profile [*Correa*, 1984].

[8] The Central Amazonia is characterized by a regime of high temperature, humidity, and rainfall. Manaus maximum daily temperature varies between 31°C and 33°C, and minimum daily temperature varies between 23°C and 24°C, showing little variability. Rainfall shows instead significant variation along the year with a minimum in August (mean rainfall, 50 mm) and a maximum in March (mean rainfall, 330), this seasonal trend being the effect of the movement of the Intertropical Convergence Zone (ITCZ). The drier season typically lasts from mid-June to mid-October but can be very variable in length and intensity [*Hodnett et al.*, 1995].

[9] The eddy covariance system [*Moncrieff et al.*, 1997] was mounted on a 41.5 m, 6.0 m cross-section tower. In order to minimize flow distortion by the tower, sensors were mounted 5 m above the tower (i.e., at a total height of 46.5 m) on its east pointing corner. The sensor is located well within the roughness sublayer of this canopy, which would be expected to extend to a height of about 1 to 2 times the canopy height (i.e., to a height of 90 m above ground level). This is not expected to significantly affect the measured fluxes as eddy covariance measurements are only weakly dependent on the applicability of surface layer similarity theory.

[10] Further details are given by *Malhi et al.* [1998].

3. Wind Direction and Fetch

[11] In sunny, daytime condition at high insolation (>500 W m^{-2}) the predominant wind direction was between northeasterly (10°–60°) in November–December and southeasterly (90°–130°) in May–June. At night there is a more uniform wind direction distribution, but still with a prevailing southeasterly direction. The body of the tower lies in the western sector (between 220° and 310°), the source of only 11% of the daytime and 18% of the nighttime winds comes.

[12] *Malhi et al.* [1998] estimated that 90% of the flux originated from forest canopy between 20 and 1840 m from the tower in the daytime covering an area of 255 ha. At nighttime the equivalent flux footprint was much larger: between 400 and 15,000 m, covering an area of 44,000 ha. However, the nighttime footprint estimates may be grossly overestimated because of the intermittent nature of nighttime turbulent transport.

[13] For more details see *Malhi et al.* [1998].

4. Instrument and Measurements

[14] Instantaneous wind velocities were measured using a three-dimensional sonic anemometer (Solent, Gill Instruments, Lymington, England). CO_2 concentrations were measured with a fast response Li-6262 infrared gas analyser (LICOR, Lincoln, Nebraska), sampling at an effective frequency of 5 Hz. The air sample was pumped at 6 dm^3 min^{-1} along 10 m of 6 mm Teflon-lined Dekabon tubing. The gas analyser analogue output signal was sent to the sonic anemometer, where it was digitized and combined with the wind data. The combined digital output was collected at 20.8 Hz on a laptop computer and fluxes were calculated in real time using University of Edinburgh Edisol software [*Moncrieff et al.*, 1997].

[15] The gas analyser was regularly calibrated using zero and fixed concentration reference gases (for CO_2), and with fixed water vapour content samples generated using a Li-Cor Li-610 dew point generator. The calibration was made on a weekly basis, and little drift in analyser concentration over a diurnal or on a week-to-week basis was observed. 10 Solarex MSX60 solar panels were used to supply the energy to all the instrumentation.

[16] The meteorological data were collected from a tower-top automatic weather station operated by INPA, at a height of 43 m above the forest floor (i.e., 3.5 m below the flux instrumentation). Soil moisture data were collected manually by INPA staff with neutron probes at three access tubes in the vicinity of the tower, at approximately biweekly frequency.

5. Data Continuity

[17] The weather data were continuous over the full annual cycle discussed here (1 September 1995 to 31 August 1996) with the only problem being occasional failure of the rain gauge, and dirty net radiometer domes

over one period (see below). There were, however, significant gaps in the flux measurements. The sonic anemometer is designed to work in all weather but gaps in data occurred because of breakdown of the analyser. 59% of the possible data between the first (16 October 1995) and last measurement date (15 August 1996) were collected, and measured flux data are available for 54% of the time over the full annual cycle. In this paper we employ an empirical gap-filling scheme to generate a full annual cycle of flux data.

[18] Gaps in the rainfall data were filled by substituting data from nearby sites at Fazenda Dimona (20 km to the north) and Rederva Ducke (40 km to the south); these substitute data appear reasonable at most periods, but the unusually low rainfall recorded in December and January (when Ducke data were used) may be the result of systematic differences caused by the proximity of Ducke to the main stem of the Rio Negro.

6. Methods

6.1. Data Processing

[19] Corrections were applied for the undersampling of high-frequency fluctuations using the approach outlined by *Moore* [1986] and *Moncrieff et al.* [1997]. Transfer functions were calculated for the loss of signal due to tube length, finite instrument response times, sensor separation and path length, and low frequency signal loss due to detrending.

[20] In an earlier paper describing the CO_2 fluxes from this site [*Malhi et al.*, 1998], fluxes were calculated after first detrending the raw data using a digital recursive filter time constant of 200s, an approach that is considered standard in many flux calculation methodologies [e.g., *Moncrieff et al.*, 1997; *Aubinet et al.*, 2000]. In recent years, however, there has been much debate on the principles of eddy covariance (J. J Finnigan et al., A re-evaluation of long-term flux measurement techniques, part 1, averaging and co-ordinate rotation, submitted to *Boundary-Layer Meteorology*, hereinafter referred to as Finnigan et al., submitted manuscript) and in this paper we have taken a new approach to flux calculation. The major new features are as follows:

1. The raw data are not detrended. It is assumed that all covariance between water vapour concentration and vertical wind velocity on timescales up to 24 hours represents genuine transport by long timescale atmospheric processes, and should not be removed from the data.

2. Previously, the raw wind speed data were ''rotated'' every 10 min (up to 2 December 1995) or half hour (after 2 December 1995) such that the mean vertical wind velocity over that 10 min or half hour period was zero. This procedure also acts as a crude ''filter'' of low frequency fluctuations. A reanalysis of the data showed that the calculated fluxes continued to increase up to rotation and averaging periods of 4 hours, but then showed no further increase in calculated flux at longer periods (see Figure 7 later). In this paper, a rotation period of 4 hours was used. There were large periods in the data where no raw data were collected and we have only the original half-hour calculated fluxes. For these data we applied a fixed multiplying factor to the originally calculated fluxes based on the observed effect of the ''low-frequency correction'' on periods when raw data still exist. The low frequency correction increased sensible heat fluxes by 43.3%, and latent heat fluxes by 32.1%, and daytime CO_2 fluxes by 30.7%.

3. A revised analysis was also applied in the correction of the effects of tube damping. In the previous analysis, a theoretical approach was used to calculate and correct for the damping of fluctuations of CO_2 and H_2O at high frequencies [*Moncrieff et al.*, 1997]. However, the damping of water vapour fluctuations is frequently observed to be greater than expected, probably because of the presence of hydrophylic impurities such as aerosols deposited on the tube walls. In the new analysis we used a more data-oriented approach, observing the damping of water-vapour fluctuations relative to CO_2 fluctuations, calculating the correction required to match the water vapour to the CO_2 (following the approach of *Hicks and McMillen*, [1988]), examining the relationship between this correction and atmospheric VPD, and calculating a general humidity-dependent correction to apply to all data. Details of the approach and its application are described by Clement et al. (manuscript in preparation). Latent energy fluxes were on average increased by 10.8% by this reanalysis.

[21] The detailed investigation of the effects of these corrections on all fluxes, and their implications for eddy covariance methodologies, is presented in a companion paper (Finnigan et al., submitted manuscript). This paper concentrates on the field measurements obtained from central Amazonia, rather than on methodological issues.

6.2. Calculation of Canopy Conductance

[22] Turbulent flux data and weather station data were used to calculate the aerodynamic resistance, r_a, using the equation:

$$r_a = \left(\frac{u}{u_*^2}\right) + \frac{1}{ku_*}\left[\ln\left(\frac{z_{oM}}{z_{oH}}\right) + \Psi_M - \Psi_H\right]$$

where r_a is the aerodynamic resistance in s m^{-1}, u and u_* are the mean horizontal wind speed and the friction velocity respectively, in m s^{-1}, k is von Karman's constant (0.41), and Ψ_M and Ψ_H are the integral diabatic correction factors for momentum and heat [*Paulson*, 1970]. Following *Garratt* [1992] we assume $\ln(z_{0M}/z_{0H}) = 2$ for uniform canopies.

[23] The measured water vapour fluxes (in kg m^{-2} s^{-1}) were used to calculate canopy resistance to water vapour, r_s by inverting the Penman-Monteith equation:

$$r_s = \frac{sr_a(R_n - \lambda E) + \rho_a c_p D}{\lambda E \gamma} - r_a$$

where r_s is the canopy resistance in s m^{-1}, s is the rate of change of vapour pressure with temperature in Pa K^{-1} (interpolated from *Monteith and Unsworth* [1990]), R_n is the net radiation in W m^{-2}; λ is the latent heat of vaporization of water in J kg^{-1}, E is the water vapour flux in kg m^{-2} s^{-1}, ρ_a is the density of dry air in kg m^{-3}, c_p is the specific heat of dry air in J kg^{-1} K^{-1}, D is the vapour pressure deficit in Pa, and γ is the psychometric constant at a given temperature, T, in Pa K^{-1}.

[24] The canopy conductance (in molar units) can then be calculated from canopy resistance [*Grace et al.*, 1995]:

$$g_s = \frac{P}{\Re T r_s}$$

where g_s is the canopy conductance in mol m^{-2} s^{-1}, P is the atmospheric pressure in Pa, R is the universal gas constant 8.314 J mol^{-1} K^{-1} and T is the air temperature in K.

[25] To ensure that wet leaf surfaces were not contaminating our estimates of g_s, data were excluded from all days where rain events occurred. Observations of leaf drying showed that most of the canopy leaf surface dried within 20 min of the termination of rainfall, whereas droplets on the leaf drip-tip remained for up to 2 hours. Because typically only about 1% of incident solar radiation reaches the soil surface [*Shuttleworth*, 1989], the contribution of soil evaporation is estimated to be less than 10 W m^{-2}, and is here neglected.

7. Results and Discussion

[26] The subsequent sections present results on a number of aspects of the data. For ease of context, discussions of the results are presented within the same sections, rather than afterward.

7.1. Meteorological Conditions

[27] Climatic conditions over the measurement year (September 1995–August 1996) are illustrated in Figure 1. All meteorological data except rainfall were continuous over this measurement period. There were several gaps in the rain data due to blockage of the rain gauge. In these periods, rain data from nearby sites at Fazenda Dimona (20 km to the north) and Reserva Ducke (40 km to the south) were used as substitutes (with the former site being the preferred option when available); these substitute data appear reasonable at most periods, but the unusually low rainfall recorded in December and January (when Ducke data was used) may be the result of systematic differences between Ducke and Cuieiras (for a discussion of local spatial variability in rainfall, see *Ribeiro and Adis* [1984]).

[28] The climate in central Amazonia shows little seasonal variation in temperature or sun angle (monthly mean maximum daily temperature in Manaus varies between 31°C in the wet season and 33°C in the dry season, minimum daily temperature between 23°C and 24°C). There are however, significant variations in rainfall, with accompanying changes in soil and atmospheric moisture content, and in cloudiness (mean August rainfall in Manaus, 50 mm; mean March rainfall, 330 mm). Total rainfall over the year was estimated to be 2088 mm.

[29] The dry season shows substantial interannual variability in its duration and intensity [*Hodnett et al.*, 1995], but typically lasts from June until October, and is associated with the northward movement of the Intertropical Convergence Zone (ITCZ) away from the equator. It is important to understand the representativeness of any measurement period in the context of 20th century climate. Figure 2 compares the measurement period with rainfall records from the nearby city of Manaus. The rainfall records cover the period 1901–1989, excluding 1909. Total annual rainfall

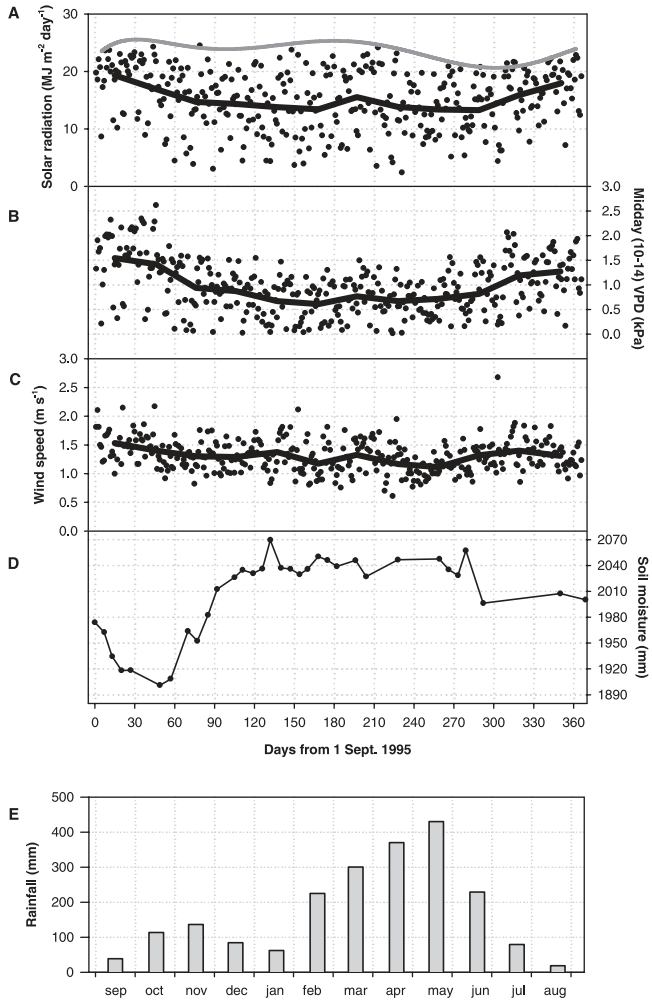

Figure 1. Variation of environmental factors over the study year, 1 September 1995 to 31 August 1996: (a) Total daily solar radiation. The points represent daily totals, the thick line plots monthly mean values, the light solid line plots maximum solar radiation assuming clear-sky conditions (see text). (b) Atmospheric (above-canopy) water vapour deficit at 43 m height, averaged between 10:00 and 14:00 local time (solid points). The solid line plots monthly mean values of the points. (c) Mean daily wind speed at 43 m height (points), and monthly means (solid line). (d) Total volumetric soil moisture content in the upper 4 m of the soil; each point represents a measurement day. (e) Total monthly rainfall. For details on gap-filling see text.

over the period ranges between 1090 and 2840 mm and shows a bimodal frequency distribution, with peaks at 2000 and 2500 mm (Figure 2a). The period mean is 2054 mm, and the median 2029 mm.; thus rainfall over the measurement period was close to the 20th century average. Rather than total annual rainfall, the number of months with rainfall less than 100 mm can be a useful indicator of water stress in tropical forests (see later). The number of dry months in Manaus can vary between 0 and 8, with mean 4.1, median 4. The measurement period had 5 dry months, this suggests that the water stress was slightly greater than average, but not unusually so. However, the rainfall in the months preceding the measurement period are also relevant. Rain-

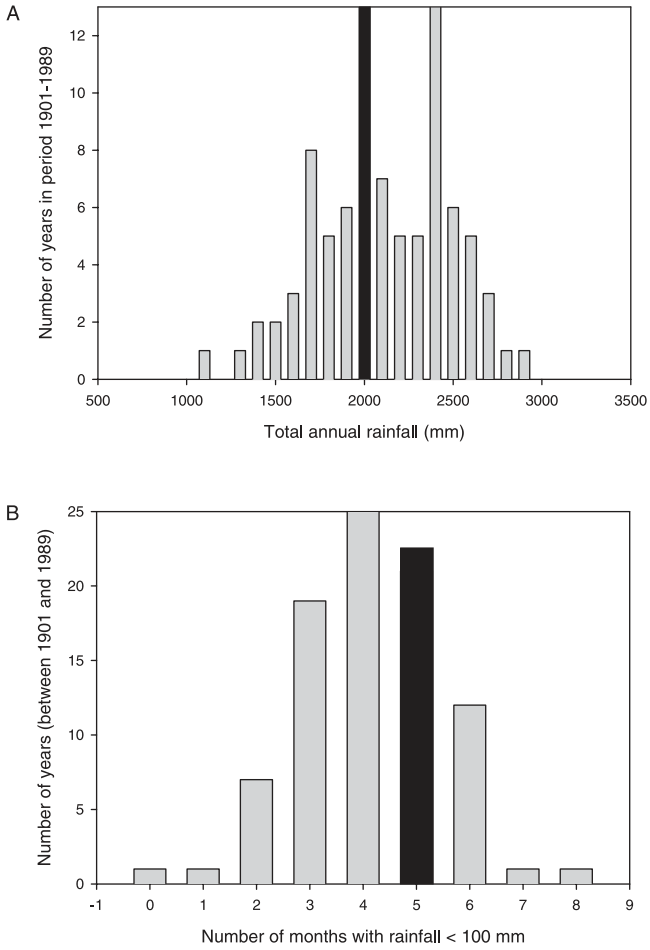

Figure 2. Frequency distribution of (a) rainfall and (b) number of dry months in the nearby city of Manaus between 1901 and 1989 (excluding 1909, when do data were collected). The value for the measurement period (September 1995 to August 1996) is shown in black. A dry month is defined has having rainfall <100 mm.

fall data for this period are not available, but the low soil water content at the start of the measurement period (Figure 1d) suggests that the preceding months had also been quite dry. Thus the 1995 dry season may have been significantly more severe than usual.

[30] The peak solar radiation on clear days is highest near the equinoxes (Figure 1a), indicating a small sun-angle effect, but in general cloudiness is a much stronger determinant of insolation. The upper curve in Figure 1a shows the potential solar radiation, which is described below. Low insolation days correlate with lower air temperature, and rainfall events cause distinct drops in soil temperature. A strong seasonality is apparent in rainfall, but there is little variation in absolute humidity over the year. However, in the dry season, reduced evaporation and increased solar insolation (Figure 1a) do induce higher air temperatures and much higher peak water vapour deficits (Figure 1c). Total soil moisture content (Figure 1d) in the upper 4 m dropped by 130 mm in the dry season; as the available water capacity in these high clay oxisols is only about 70 mm m^{-1}, this indicates that the available water reservoirs in the upper soil were significantly depleted. The early part of the 1996 dry season was much less severe than that of 1995, with soil moisture only dropping by 20 mm by September 1996.

7.2. Radiation Balance

[31] The mean diurnal cycle of radiation in the peak dry (September–October) and wet (January–March) seasons is shown in Figure 3. Due to reduced cloudiness, mean peak solar radiation is higher by 150 W m^{-2} in the dry season, and typically peaked between 1000 and 1100 Local Time, because of increased cloudiness in the afternoon induced by the growth of the convective boundary layer. In the wet season the peak in solar radiation was biased slightly toward the afternoon, suggesting that the cloudiness was more related to large-scale weather patterns (such as squall lines arriving from the east) rather than to the small-scale local systems typical of the dry season. There is negligible variation in day length over the year.

[32] Due to the higher solar insolation, net radiation, R, is higher in the dry season than in the wet season, but is a smaller fraction of total insolation (see below).

[33] The net long-wave radiation, L, is determined as the residual of the other terms, such that $R = S(1 - \alpha) + L$, where R is the net radiation, S is total incoming potential solar radiation, α is the albedo and $1 - \alpha$ is the surface solar absorbance. In the dry season, L shows a smooth mean diurnal cycle, closely following canopy temperature and peaking at -70 W m^{-2} (negative values indicate a net loss of thermal radiation from the surface to the atmosphere); in the wet season the diurnal amplitude is much lower, though there is a peak in the late afternoon suggesting that the lower atmosphere cools more rapidly than the forest canopy. Nighttime values of L are also smaller in the wet season. The variation in L is related to cloudiness and surface temperature: in the dry season the downward component of long-wave radiation is decreased (more of the atmospheric thermal emission emanates from the middle troposphere rather than from warmer cloud bases) and the upward component is increased (the canopy is warmer

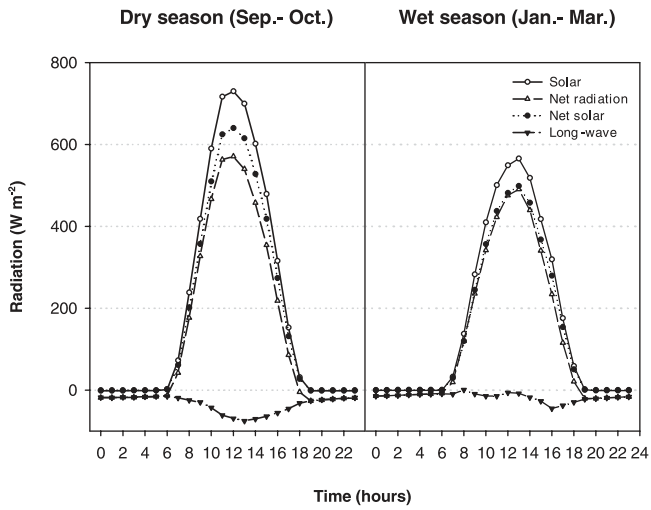

Figure 3. Mean diurnal radiation budget for two periods: dry season (September–October 1995), and wet season (January–March 1996).

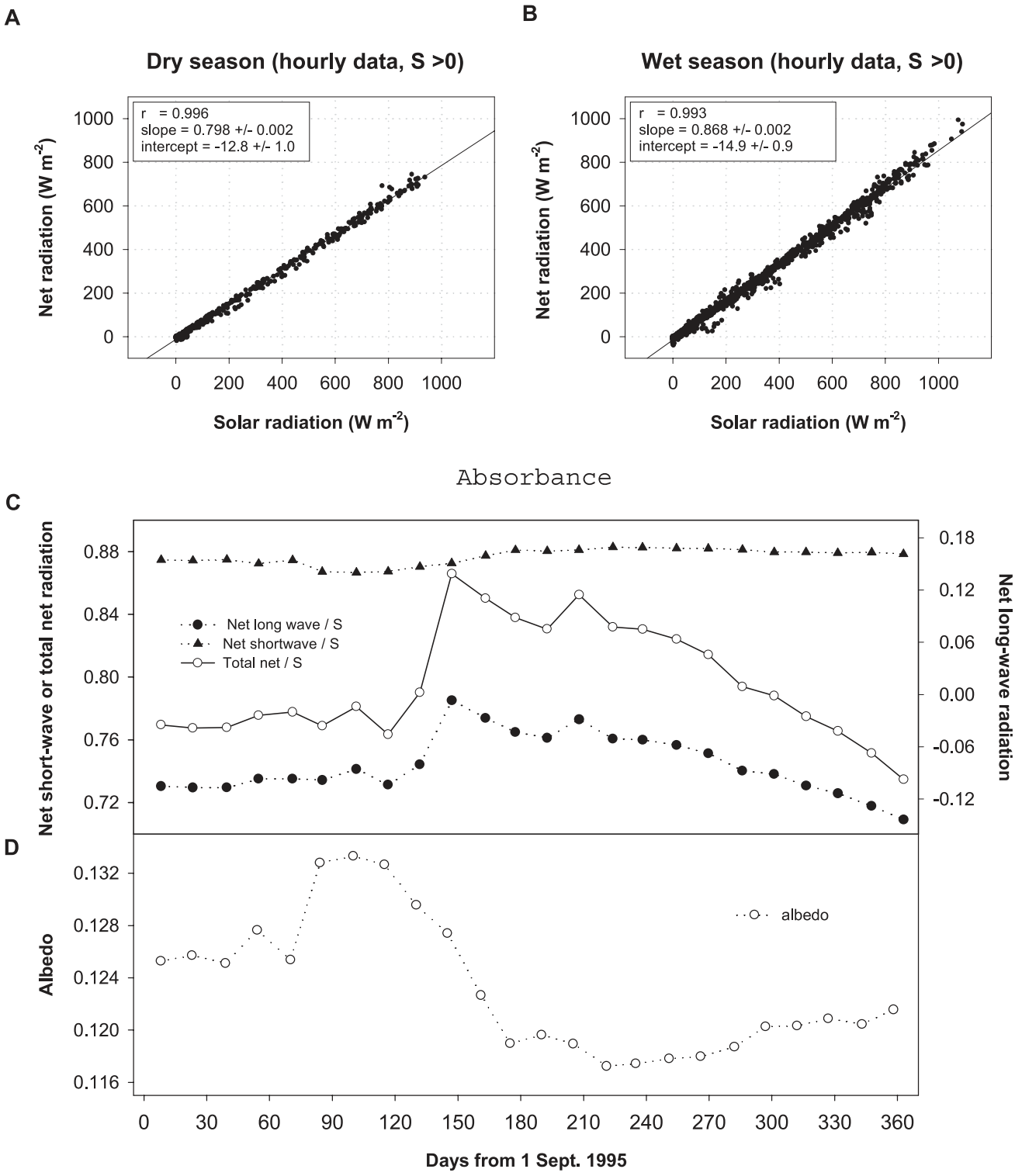

Figure 4. The relationship between net (shortwave + longwave) radiation and short-wave incoming solar radiation in peak dry season (mid-October-mid-November: Figure 4a) and wet season (January–March: Figure 4b). The errors quoted are 95% confidence limits. (4c) 15-day means of the short and long-wave components of the net radiation budget plotted as fractions of incoming solar radiation: net long-wave radiation (scale on right-axis), net solar shortwave radiation (= 1−albedo) and total net radiation. All values are derived as gradients from plots such as those shown in Figures 4a and 4b. (15d) 15 day mean values of measured canopy albedo, derived from plots of reflected solar radiation against incoming solar radiation.

because of increased solar insolation and reduced evaporation due to soil moisture limitation). Hence the net downward thermal radiation flux in the dry season is more negative than in the cloudier, cooler wet season.

[34] The relationship between short-wave and net radiation is linear with little scatter, with the slope varying between wet season (Figure 4a) and dry season (Figure 4b). In fact, we took any variation from this linear relationship as an indicator of contamination of the net radiometer domes. Between 17 December 1995 and 7 January 1996 the net radiation showed consistently low readings which disappeared when the net radiometer domes were changed; for this period we calculated a ''corrected'' net radiation by assuming that $R = 0.79 \times S$.

[35] Figures 4c and 4d show 15-day means of the components of the radiation budget plotted as fractions of incoming solar radiation. These were determined from the gradient of the plot of each component against S, as shown in Figure 4a for R, and are therefore dominated by the daytime relationship between these variables. The albedo is higher in the dry season, peaking at 13.2% at the start of the wet season in December. The timing of the peak suggests that this variation is more related to leaf phenology (minimum leaf area and/or growth of new leaves) than directly to plant water status. The albedo reaches a broad minimum value of 11.8% in the second half of the wet season. Any individual tower-based albedo measurement can be unreliable, as the sampling area may be overly influenced by the seasonal phenology of an individual tree, but *Culf et al.* [1995] report a very similar pattern in albedo at three other tower sites across Amazonia. They found that the albedo variations were strongly correlated to soil water content, and not correlated to cloudiness.

[36] The range of variation of R (a range of 8% of incoming solar radiation) is much larger than the variation in albedo (a range of only 1.4% of incoming solar radiation), and is largely explained by variations in L. Hence the long-wave radiation balance is a more important determinant of seasonal variations of the radiation balance than the albedo.

[37] We calculated the total potential solar radiation at this site by using an astronomical calculation program (by *Beer* [1990]) and assuming an atmospheric transmissivity of 0.75 [*Beer*, 1990]. The potential solar radiation closely follows the upper envelope of measured solar radiation, corresponding to cloud-free days (see Figure 1a). The potential solar radiation shows a weak minimum in December and a stronger minimum in June, corresponding to the solstices, when the solar zenith angle at noon is greatest. The June minimum is deeper because the Earth-sun distance is greatest in July, and also because the site is slightly south of the equator. We calculate a total potential annual insolation of 8.63 GJ. The measured insolation for this year was 5.56 GJ; thus cloudiness reduces incoming solar energy by 35.6% below potential. The maximum reduction is about 50% in February, and the minimum reduction is 20% in August. We can also calculate the effect of sun angle by examining the peak values in September and March (when the Sun is directly overhead at noon) and multiplying these over the year. If the Sun was in ''permanent near-equinox'', potential annual solar insolation would be 9.3 GJ, higher by 7%. Thus at this tropical forest site (and probably at most tropical sites), cloudiness is a much more important determinant of the variation of insolation than sun-angle and day-length. This situation differs markedly from that in high latitudes.

7.3. Energy Balance

7.3.1. Relationships Between Daytime Fluxes

[38] The relationships between turbulent fluxes of heat and net radiation are demonstrated in Figure 5, with 5a plotting LE against R, and 5b plotting H against R. For latent energy, the slope is greatly reduced in the dry season (0.38 compared to 0.65 in the wet season), indicating that the water supply is significantly restricted. There is also greater scatter in the points in the dry season, as the rate of evaporation is more sensitive to rapid variations in soil moisture status after rains. There is some nonlinearity in the relationship in both seasons, with disproportionately high evaporation rates at high radiation levels. This may be due to increased evaporative demand associated with high leaf temperatures and atmospheric water vapour deficits (Figure 5c), although it would be expected that in such situations stomatal conductance would reduce evaporation to prevent excessive water loss. The sensible heat flux (Figure 5b) shows a similar relationship to net radiation, but with increased values in the dry season, as would be expected if evaporation rates are restricted. Again, turbulent flux values at high levels of net radiation are disproportionately high, and there is greater scatter in the dry season.

[39] The slope of the relationship between LE and R, and between H and R, were calculated for each 15 day period for which data were available, and Figure 5d shows how this slope varied over the year. There is a rapid increase in measured evaporation between mid-October and mid-December (day 50 to 100), a transition that is in almost exact synchrony with the increase in soil moisture noted in Figure 1d. From mid-December onwards the soil moisture levels saturate, and evaporation remains fairly constant until mid June (day 290) at about 0.75 of net radiation (0.6 of solar radiation). After mid-June, both soil moisture levels and evaporation rates begin to decline as the new dry season commences. The soil moisture data suggest, however, that this subsequent dry season (1996) was not as severe as the prior one (1995).

[40] A polynomial trend line was fitted through each 15-day mean value of H/S and LE/S to generate an empirical description of the variation of these parameters over the year (shown in Figure 5d). These trends were then combined with the hourly solar radiation data to produce a complete gap-filled data set of the hourly variation of H and LE over the year.

[41] The sum of H and LE (normalized by dividing by S) is also plotted in Figure 5d. This ranges between 0.7 and 0.9, with a mean value of 0.78, almost exactly matching net radiation (also 0.78). However, this ''complete'' energy balance closure does not include the storage of sensible and latent heat in plant biomass and within-canopy airspace.

7.3.2. Energy Balance Over Full 24-Hour Periods

[42] The graphs in Figure 5d largely reflect the daytime energy balance, when the canopy is accumulating heat. However, the heat gained in the day is released at night through thermal radiation and evaporation, and hence over

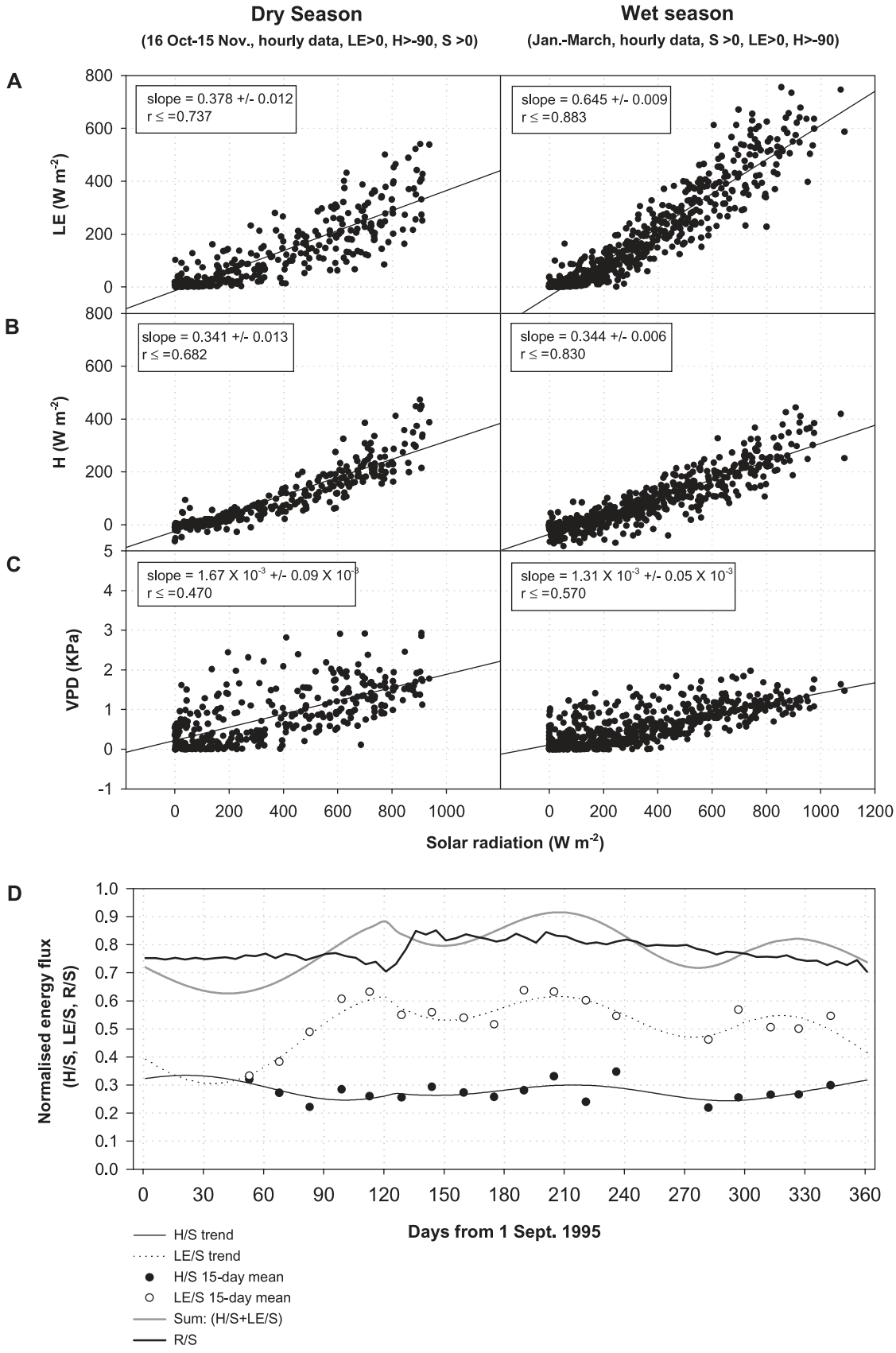

Figure 5. The relationships between (a) the turbulent latent heat flux, LE, and net radiation, *R*; (b) the turbulent sensible heat flux, H, and net radiation, *R*; (c) the atmospheric water vapour pressure deficit (VPD) and R. (d) 15-day values of H, LE, (H + LE), and *R*, calculated from plots of the variable against incoming solar radiation *S*. Note that (H + LE) is close to *R* for much of the year.

24 hours the heat storage term sums to approximately zero and can be neglected. Hence, by comparing the day-time energy balance closure with the full 24-hour energy, balance closure, we can estimate the magnitude of the canopy heat storage term. Figure 6 plots the 24-hour totals of H, LE and *R*. Now the annual mean value of (H + LE) is 136.4 W m^{-2}, equivalent to 105% of the annual mean of net radiation (129.8 W m^{-2}), thus we can estimate that, on average, the daytime accumulation of heat within the canopy accounts for approximately an extra 5% of daytime *R*, or 7 W m^{-2}. This is only an approximate estimate, as it includes periods where the fluxes were empirically filled and hence not a reliable measure of the nighttime fluxes. The Bowen Ratio (= H/LE) varies between 0.5 in the wet season and 1.1 in the peak dry season (late September), with an annual mean value of 0.58.

[43] The overall energy balance closure at this site is extremely good (within 5%), giving a high degree of confidence in the flux measurements. Many flux studies over forests have tended to not achieve energy balance closure. For example, *Aubinet et al.* [2000] presented the energy balance results from six EUROFLUX sites. Closure varied from 99% in the best case to 70% in the worst. For tropical forests, *Shuttleworth et al.* [1984] reported a total energy balance closure of 93% for eight days of measurements. However, most tropical forests sites within the LBA (Large-Scale Biosphere Atmosphere Experiment in Amazonia) are reporting closure to only within 70–80%. An important difference in the current analysis is that we have included flux transport at timescales of 1 to 6 hours, which are usually neglected in flux calculations. If these longer timescales are ignored, using the same analysis procedure as that applied by *Malhi et al.* [1998], the energy balance closure would only be 77%, within the usual range for forests. The variation of energy balance closure with averaging period is demonstrated in Figure 7. Only the subset of data in unbroken 12-hour periods was included in the analysis shown in this figure, resulting in slightly different values of energy balance closure. Energy balance closure improves to approximately 100% when an averaging period of 4 hours is used, but shows no further significant variation when longer averaging periods are used.

[44] The high-frequency water vapour correction accounts for a 6% increase in energy balance closure (i.e., from 77% to 83%), and the low-frequency correction accounts for a 22%

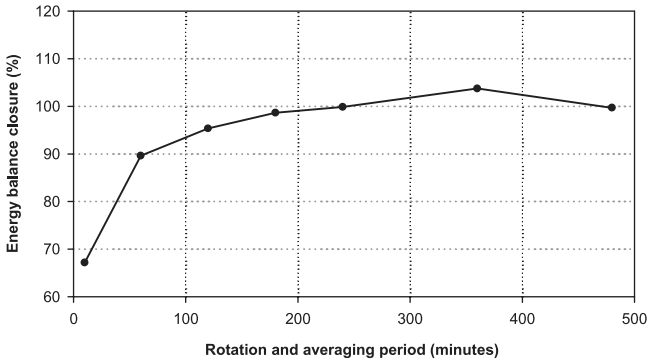

Figure 6. The variation of energy balance closure (%) with increasing rotation/averaging period (in minutes).

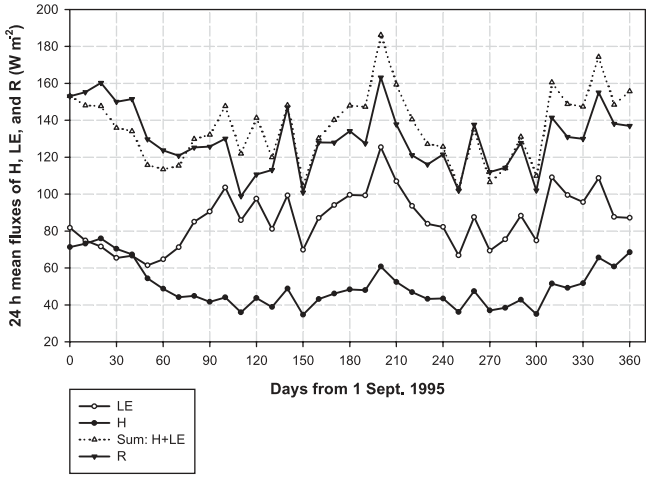

Figure 7. Fluxes summed over the full 24 hour cycle, and shown as ten-day means: sensible heat flux, H, latent heat flux, LE and net radiation, *R*, with gap-filled values of H and LE being used where field data do not exist. The gap-filling procedure is described in the text.

increase (from 83% to 105%). This result strongly suggests that, for this site at least and potentially for other forest sites, the problem of poor energy balance closure may be solved by considering flux transport at longer timescales. It also suggests that daytime fluxes over forests have often been underestimated. The nature of flux transport at low frequencies is discussed by Finnigan et al. (submitted manuscript).

[45] There appears to be a moderate seasonal pattern in energy balance closure, with closure varying from about 95% in the dry season to 105% in the wet season. Poorer energy balance closure (i.e., greater underestimation of turbulent) in dry conditions has been noted in a number of other studies. The reason for greater underestimation in the dry season is not clear: it would perhaps be expected that increased likelihood of liquid water on the sensors would reduce the measured fluxes in the wet season.

7.3.3. The Diurnal Cycle of Energy Fluxes

[46] The mean diurnal cycles of the energy fluxes in the dry and wet season are shown in Figure 8. This includes an estimate of the energy consumed in photosynthesis and released in respiration. This was calculated from the diurnal cycle of carbon exchange reported by *Malhi et al.* [1998], using the fact that 468 kJ of energy are required for the photosynthesis of 1 mole of CO_2 into glucose [*Grace*, 1983]. Thus a CO_2 flux of 1 μmol m^{-2} s^{-1} requires an energy flux of 0.468 W m^{-2}. Hence, the forest photosynthesis consumes approximately 12 W m^{-2} during peak insolation (1.8% of solar radiation, or 2.3% of net radiation), and continuously releases about 3.3 W m^{-2} through autotrophic and heterotrophic respiration.

[47] An estimated hourly "canopy storage" term is calculated as the residue between net radiation and the sum of the hourly latent, sensible and photosynthetic energy fluxes (which have been corrected using the 24-hour energy balance). In the peak dry season the measured energy balance closure is still rather poor (84%) and hence the canopy storage term is overestimated; in the wet season period shown (only part of the total wet season) the energy

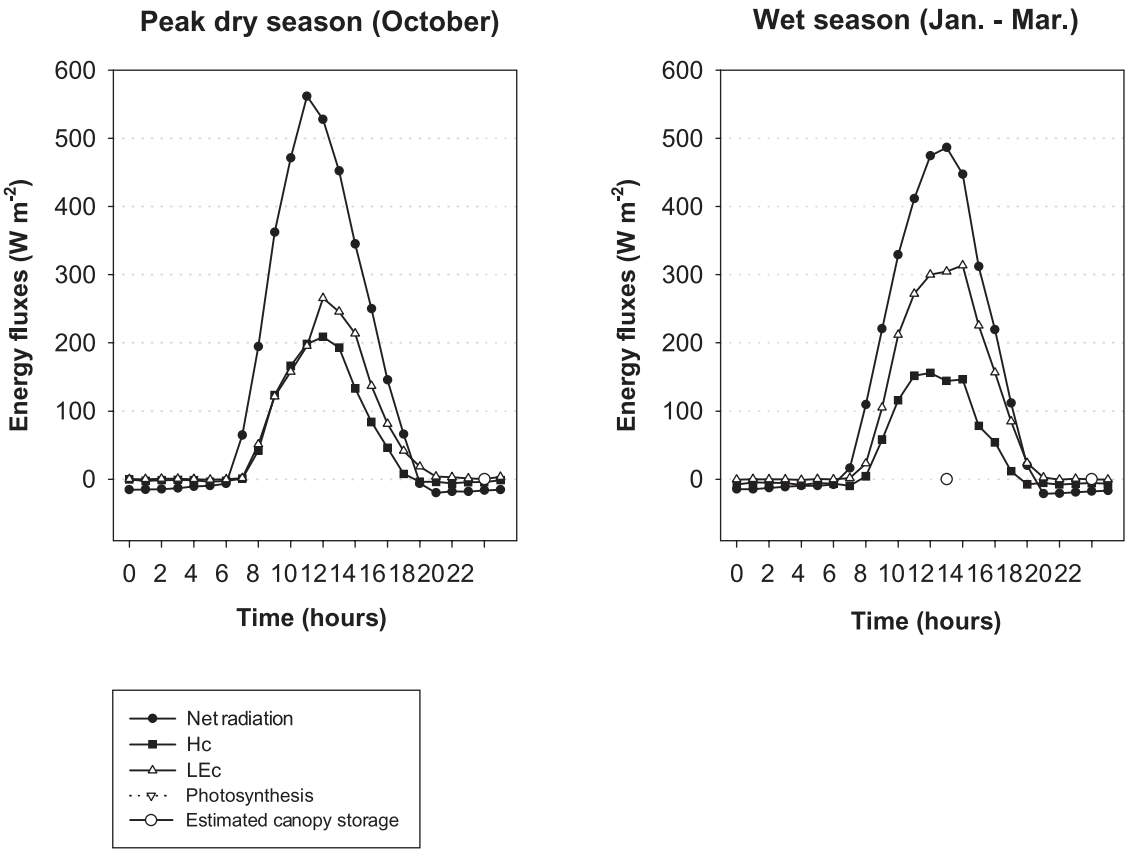

Figure 8. The mean diurnal cycles of the energy fluxes in the peak dry season (15–30 October 1995) and wet season (January–March 1996). The canopy storage flux is estimated as a residue of the other terms.

balance closure is good (96%). Using stem and air temperature and humidity measurements, *Moore and Fisch* [1986] estimated the early dry season canopy heat storage in the nearby Ducke forest to peak at 60–80 W m^{-2} in mid morning. This storage term was approximately equally partitioned between canopy airspace heat storage, canopy airspace humidity increases and biomass temperature increase. The peak dry season value of 180 W m^{-2} (Figure 8) is therefore larger than expected (consistent with the lack of 24-hour energy balance closure), but the wet season value of 50 W m^{-2} is close to that expected. In both seasons the energy balance residual peaks in midmorning and zero by midafternoon, as would be expected if it were a canopy storage term.

[48] The peak latent heat flux appears to be slightly higher in the wet season (300 W m^{-2}) than in the dry (250 W m^{-2}), despite the reduced net radiation. Conversely, the peak sensible heat flux increases from 150 W m^{-2} in the wet season to 220 W m^{-2} in the dry, because of the increased radiation load and reduced transpiration.

7.4. Annual Energy Budget

[49] The annual and seasonal energy budgets for this forest site are summarized in Table 1. Here the wet season

Table 1. Summary of the Annual and Seasonal Energy Budgets[a]

Radiation Components	Year Total, GJ m^{-2} yr^{-1}	(Scaled to Energy Balance Closure)	Dry Season, MJ m^{-2} d^{-1}	Wet Season, MJ m^{-2} d^{-1}	Difference, MJ m^{-2} d^{-1}
Solar (clear sky)	8.63 (155%)		24.66 (135%)	24.9 (173%)	−0.2
Solar (incident)	5.56 (100%)		18.3 (100%)	14.4 (100%)	3.9
Solar (absorbed)	4.93 (89%)		16.1 (88%)	12.66 (88%)	3.4
Long wave (net emission)	0.83 (15%)		3.15 (17%)	1.45 (10%)	1.7
Net radiation	4.1 (74%)		12.95 (71%)	11.21 (78%)	1.7
Sensible heat	1.58 (28%)	1.49 (27%)	5.85 (32%)	4.01 (28%)	1.8
Latent heat	2.73 (49%)	2.58 (46%)	6.91 (38%)	8.25 (57%)	−1.3
Net carbon fixation	0.03 (0.5%)	0.03 (0.5%)	0.07 (0.4%)	0.08 (0.6%)	−0.01

[a] Here, the wet season period covers January to March, and the dry season covers August to October (thus actually covering parts of two dry seasons). The figures are also shown as percentages normalized to measured incoming solar radiation at the surface.

Table 2. Annual Variation of the Forest Water Budget Plotted as 15-Day Averages[a]

Start of 15-Day Period	Approx. Period	Net Radiation *R* Equiv ent, mm	Rainfall *P*, mm	Evaporation *E*, mm	Soil Moisture, 0–4 m mm	Soil Mist Deficit, mm	Midday VPD, kPa	Maximal Evaporation, E' mm	E/R	E/E'
0	early Sept.	77.78	10.4	40.19	1974	−76.0	1.94	66.11	0.52	0.61
15	late Sept.	85.13	28.4	37.99	1930	−120.1	1.82	72.36	0.45	0.53
30	early Oct.	80.86	25	34.66	1916	−133.8	1.81	68.73	0.43	0.50
45	late Oct.	74.41	35.4	34.18	1904	−145.7	1.49	63.25	0.46	0.54
60	early Nov.	63.20	139.2	33.32	1921	−128.8	0.97	53.72	0.53	0.62
75	late Nov.	69.92	48	45.22	1956	−94.4	1.16	59.43	0.65	0.76
90	early Dec.	68.48	36.87	50.08	2004	−46.1	0.97	58.21	0.73	0.86
105	late Dec.	59.22	48.02	49.52	2026	−23.6	0.89	50.34	0.84	0.98
120	early Jan.	54.89	30.61	46.21	2032	−18.3	0.76	46.66	0.84	0.99
135	late Jan.	78.56	26.9	52.66	2057	7.4	0.89	66.78	0.67	0.79
150	early Feb.	58.67	61.57	39.77	2033	−16.7	0.66	49.87	0.68	0.80
165	late Feb.	69.78	147.6	49.50	2045	−5.1	0.82	59.31	0.71	0.83
180	early March	70.81	155.6	52.37	2041	−9.0	0.78	60.19	0.74	0.87
195	late March	82.10	75.8	62.97	2045	−4.5	0.98	69.79	0.77	0.90
210	early April	65.05	328.2	50.05	2032	−17.9	0.69	55.30	0.77	0.91
225	late April	69.92	132.74	51.09	2044	−5.8	0.82	59.43	0.73	0.86
240	early May	59.48	15.89	39.70	2047	−3.1	0.63	50.56	0.67	0.79
255	late May	70.46	307.4	44.45	2047	−2.6	1.02	59.89	0.63	0.74
270	early June	56.74	259.6	35.01	2031	−18.5	0.67	48.23	0.62	0.73
285	late June	70.73	75.59	47.94	2029	−20.8	1.23	60.12	0.68	0.80
300	early July	64.49	24.68	47.93	1998	−52.2	1.32	54.82	0.74	0.87
315	late July	70.27	56.4	52.87	2001	−49.4	1.42	59.73	0.75	0.89
330	early Aug.	76.59	0	55.29	2004	−46.5	1.47	65.10	0.72	0.85
345	late Aug.	75.73	18.8	48.60	2006	−43.6	1.47	64.37	0.64	0.76
360	late Aug.	34.72	0	21.85	2003.6	−46.4	1.59	29.51	0.63	0.74
Total or Mean		1707.98	2088.67	1123.43	2005	−44.86	1.13	58.07	0.66	0.78

[a] The columns are equivalent total net radiation, *R* (millimeters), total rainfall, *P* (millimeters), estimated evaporation, *E*, soil moisture content in upper 4.0 m (millimeters), soil moisture deficit (millimeters), midday water vapor pressure deficit (kilopascals), maximal evaporation, E' (defined in text: millimeters), evaporative fraction, E/R, and the ratio between evaporative and maximal evaporation, E/E'.

period covers January to March, and the dry season covers August to October (thus actually covering parts of two dry seasons). The figures are also shown as percentages normalized to measured incoming solar radiation at the surface.

[50] Over this year, 35.6% of potential surface insolation was intercepted by clouds, with this proportion being higher in the wet season (42.2%) compared to the dry season (25.8%). Seasonal variation in albedo has an almost negligible influence on surface energy balance over the year, but the surface loses much more energy as net long-wave emissions in the dry season, when the vegetation is hotter (more sun, less water) and the skies are sunnier and less cloudy (less thermally insulating). Overall, the net (long-wave + short-wave) radiation at the surface is 15% greater in the dry season than the wet, but this difference is less than half of what would be expected from consideration of sunshine alone, because of the compensating effect of the long-wave radiation losses.

[51] It is unlikely that seasonal variation in leaf area index has a significant affect on the radiation balance. *Williams et al.* [1998] conducted a sensitivity study for this site that suggested that above LAI values of 4 almost all of the available energy is already being intercepted by the canopy. Variations in LAI above this threshold have a negligible effect on energy balance; LAI in this tropical forest canopy is estimated to vary between 5 and 6.

[52] The net radiation is energy that is available for evapotranspiration, sensible heat convection and photosynthesis. We assume that net heat storage in the canopy and soil are negligible over the full annual cycle. In an equilibrium forest, the overall energy usage by photosynthesis should be balanced by that released by respiration. However, *Malhi et al.* [1998] estimated that the site was a carbon sink of 5.9 t C ha^{-1} yr^{-1}. This value is perhaps implausibly high, but as an upper limit it suggests that 0.023 GJ yr^{-1} are consumed in net carbon production, a negligible amount of the annual energy budget. The sensible and heat are probably slight overestimates as the calculated energy usage of this site (including photosynthesis) was 105% of net radiation. The forest is almost continuous for hundreds of miles upwind of the tower and it is unlikely that advection is an extra energy supply at this site. The second column of Table 1 presents slightly adjusted values of the turbulent fluxes, scaled down in proportion to produce 100 % energy balance closure.

[53] Over the year, overall evapotranspiration used 66.6% of net available energy (unadjusted values), with this proportion going from 54.4% in the dry season to 73.6% in the wet season. In absolute terms, evapotranspiration was 1.34 MJ day^{-1} greater in the wet season; hence in this year the combined effects of long-wave radiation loss and reduced plant water use combined to more than offset the 3.9 MJ day^{-1} advantage the dry season had in terms of available sunshine for evaporation. The long-wave radiation term (itself influenced by plant drought stress) was slightly the more important term.

7.5. Annual Water Budget and the Effect of the Dry Season

[54] The annual variation of the water budget is summarized in Table 2, which shows 15 day averages. The total soil moisture content between 0.0 m and 4.0 m is also shown,

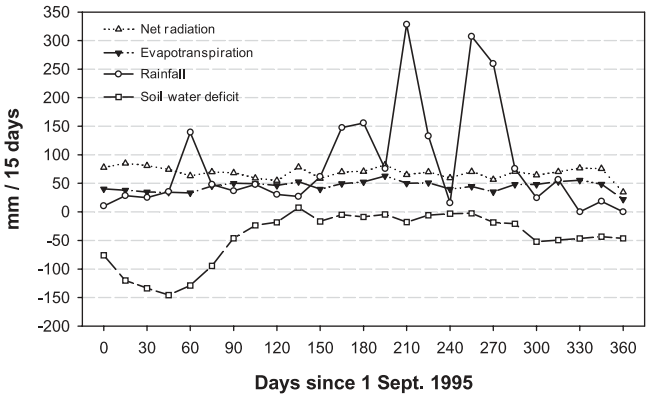

Figure 9. Forest water balance: 15-day totals of precipitation (mm), estimated evaporation (mm) and net radiation (mm water equivalent), and interpolated soil water deficit (mm in top 4 m) over the measurement period.

and the soil moisture deficit is calculated by subtracting soil moisture content from the maximum value during the dry season, when the soil is saturated.

[55] Soil moisture status begins to decline as soon as precipitation rates drop below evapotranspiration. The threshold evaporation value is close to 50 mm per 15 day period, or 3 mm day^{-1}, or 100 mm month^{-1}. This provides a general water stress indicator that can be related to long-term precipitation records. The duration of the dry season is sometimes defined as the period for which P < 100 mm. In fact, the forest takes some time to recharge its soil moisture reserves (approximately 60 more days in this case) after the onset of the new wet season. Thus the "ecophysiological" dry season is about 60 days longer than the "meteorological" dry season.

[56] Figure 9 shows a plot of evaporation, precipitation and net radiation over the entire year. Under fully wetted conditions, evapotranspiration accounts for 75–85% of R, but this ratio declines during the dry season, and also apparently during short dry spells in the wet season. There are some discrepancies between the rainfall and soil moisture data. For example, in December and January (days 90 to 150), measured rainfall rates are low but soil moisture levels are still climbing. Similarly, in August (days 330–360) rainfall rates are declining but soil moisture remains constant. As mentioned above, in both these periods the rain gauge at the tower was malfunctioning at rain data from nearby stations was used. It is possible that local rainfall was higher at the flux site, and hence the annual totals of rainfall are underestimated.

[57] Figure 10a plots the relationship between E/R and soil moisture deficit over the year, using 15-day averaged data. During the drying phase E/R declines linearly with soil moisture, reaching a value of 0.45 in the peak dry season. Evaporation rates began to decline immediately (within 15 days) at the onset of soil water deficit, indicating that the forest is rapidly affected by water stress. During the wetting phase of the dry season, the increase in E/R is also linear with soil moisture deficit, but with higher values of evaporation. For equivalent soil moisture status, the forest is less stressed in the wetting phase of the dry season than in the drying phase. This may reflect a response to water vapour deficit, which is higher during the early dry season (Figure 10b), and possibly a throughflow of rainwater that is being used for transpiration while not being sufficient to recharge soil water stocks. There is no

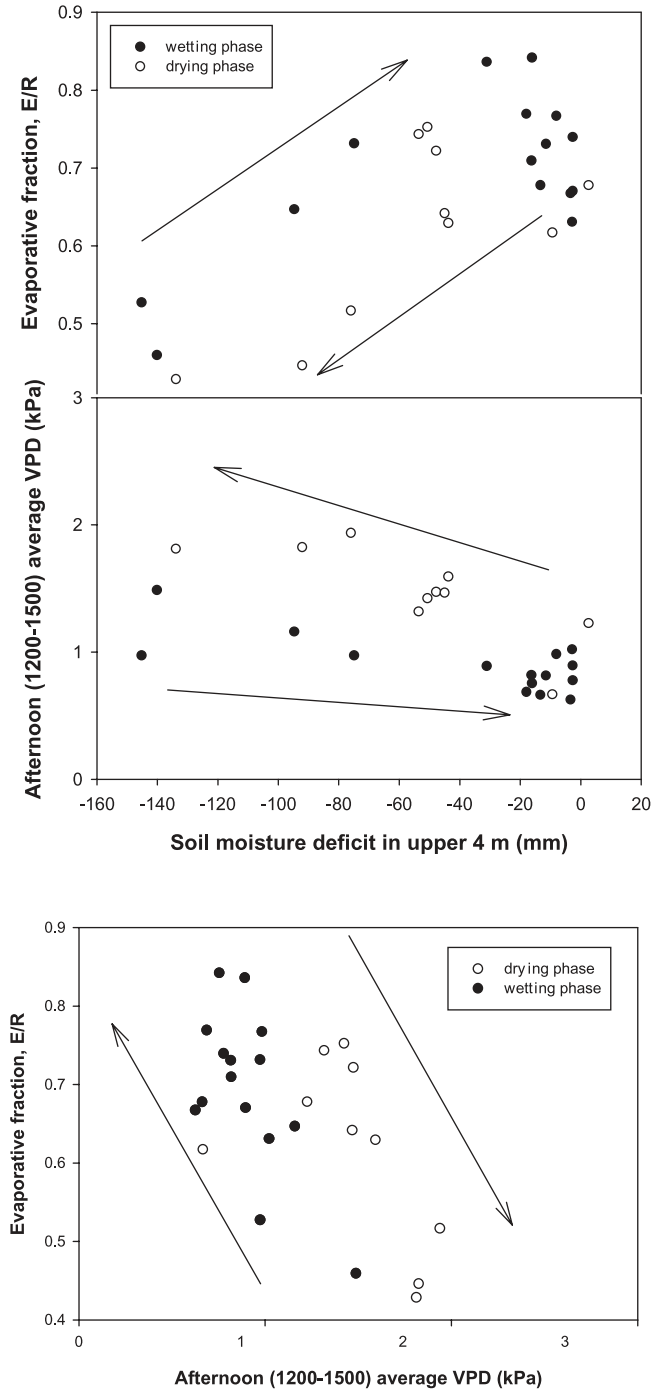

Figure 10. The relationship between (a) evaporative fraction (E/R) and soil moisture deficit, and (b) 1200–1500 water vapour pressure deficit and soil moisture deficit over the year, using 15-day averaged data. The soil moisture measurements were linearly interpolated to the middle of each 15-day period. Open circles indicate the drying phase of the seasonal cycle (soil moisture decreasing), and solid circles the wetting phase.

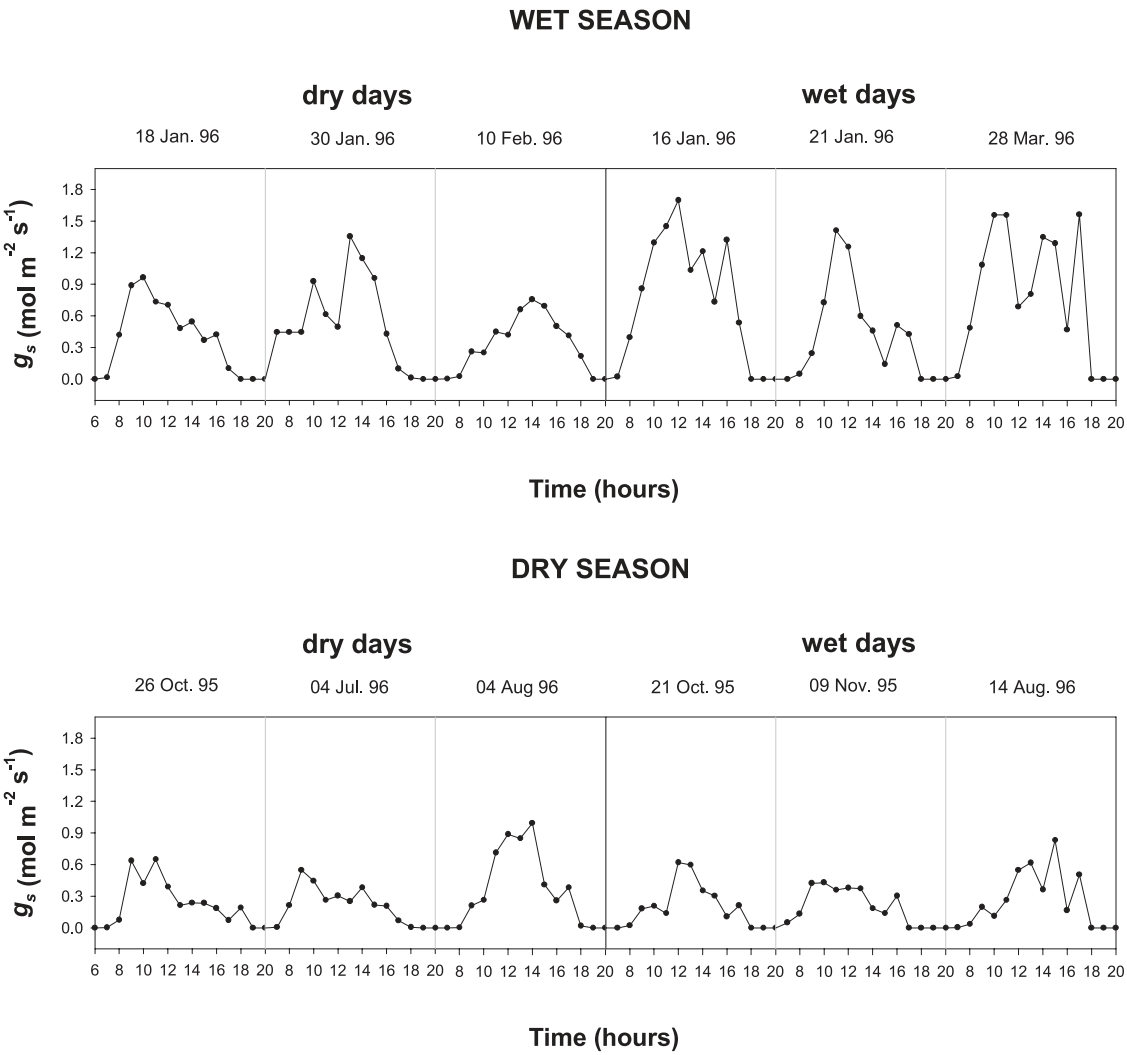

Figure 11. Calculated canopy conductance, g_s, for a selection of dry days and wet days in both wet and dry seasons. See text for definition of wet and dry days.

evidence that this dry season hampered the forest's ability to transpire in the subsequent wet season (e.g., through leaf shedding). The direct relationship between evaporative fraction and afternoon VPD is plotted in Figure 10c.

[58] The total evapotranspiration over the year was calculated to be 1123 mm yr^{-1}, 54% of precipitation (2089 mm) and 67% of net available energy. This is equal to a mean daily rate of 3.1 mm day^{-1}. This value compares with the value of 3.6 mm day^{-1} calculated by *Shuttleworth* [1989] using a Penman-Monteith approach, and a value of 4.1 mm day^{-1} calculated from streamflow measurements and water balance calculations in the same local watershed between 1981 and 1983 [*Leopoldo et al.*, 1995]. Given the good energy balance closure, it is unlikely that evapotranspiration is being underestimated by 1 mm day^{-1}, perhaps suggesting that the watershed water balance approach misses a significant amount of groundwater flow, or else that valley-bottom forest has a significantly greater evapotranspiration rates.

[59] A "maximal" evaporation was calculated by applying the range of wet season values of E/R (0.75–0.85) over the entire dry season, i.e., assuming that there is no limitation on evapotranspiration in dry period. The "maximal" evaporation over the year would have been 1280–1450 mm (3.5–4.0 mm day^{-1}). Thus the overall effect of the dry season on annual forest evapotranspiration is modest, reducing total annual evapotranspiration by 13–23%. In the peak dry season, however, the effect is severe, with evapotranspiration reduced by 43–50% below maximal, probably resulting in a further drying of local climate. This observed seasonality in evapotranspiration correlates well with the seasonality in photosynthesis described by *Malhi et al.* [1998], and the annual patterns of litterfall [*Luizão and Shubert*, 1989] indicate that there is a significant dry season effect on vegetation.

7.6. Canopy Conductance

[60] Calculated values of g_s for a selection of dry days (selected as days with no rain following at least two dry days, and not close to heavy rain events) and wet days (selected as days following two or more days with heavy rain, but still with no rain on the selected days themselves) in both wet and dry seasons are shown in Figure 11. There is significant day-to-day variation, but peak values are

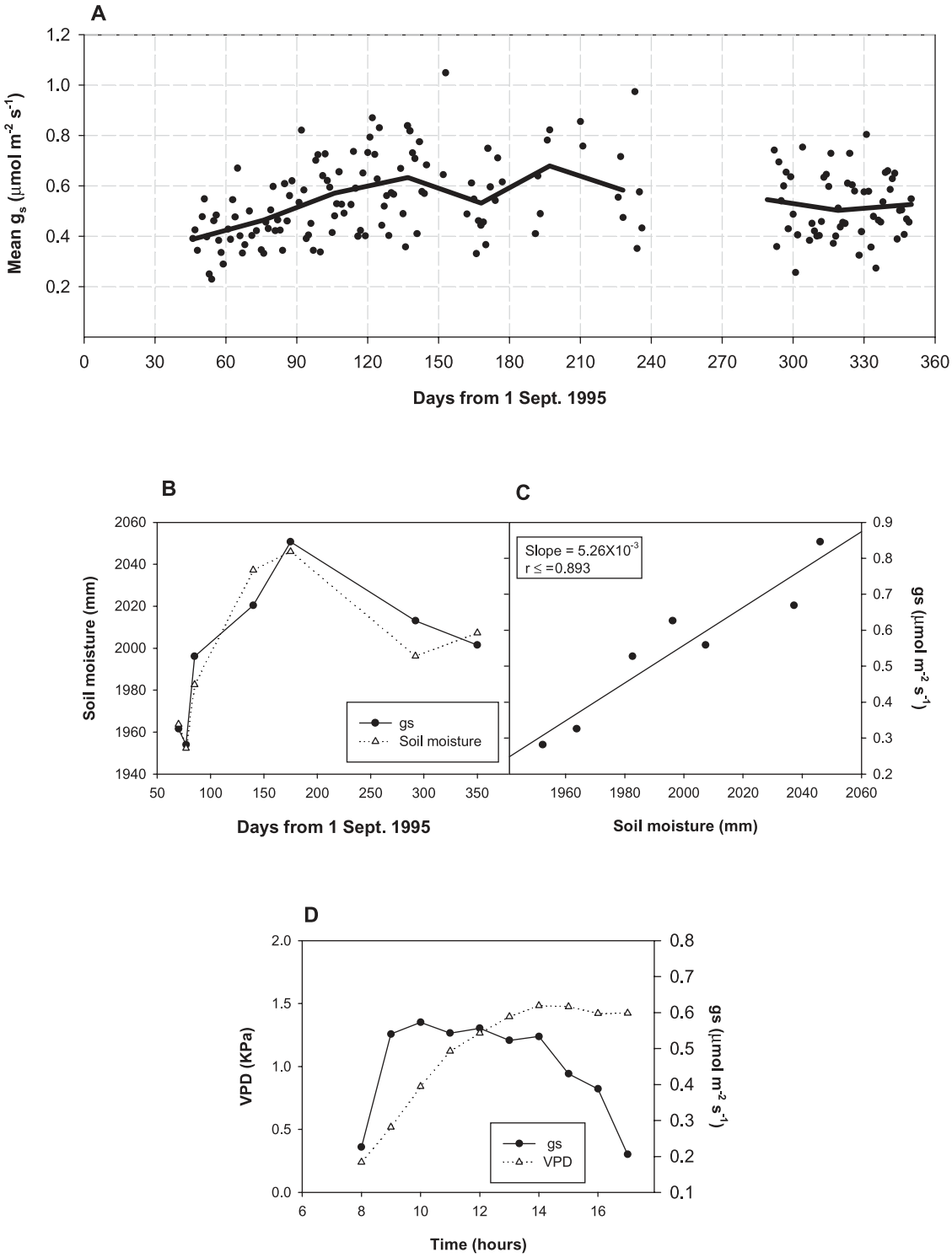

Figure 12. (a) The annual variations in mean daytime canopy conductance, and in air water vapour deficit. The conductances were only calculated for hours with high solar radiation (>400 W m^{-2}) on days without rain. (b) Canopy conductance, g_s, and soil moisture on a select number of days over the year where direct evapotranspiration flux measurements coincided with bi-weekly soil moisture measurements. (c) For the same select days, g_s plotted against soil moisture content. (d) The mean diurnal cycles of g_s and water vapour pressure deficit averaged over the year.

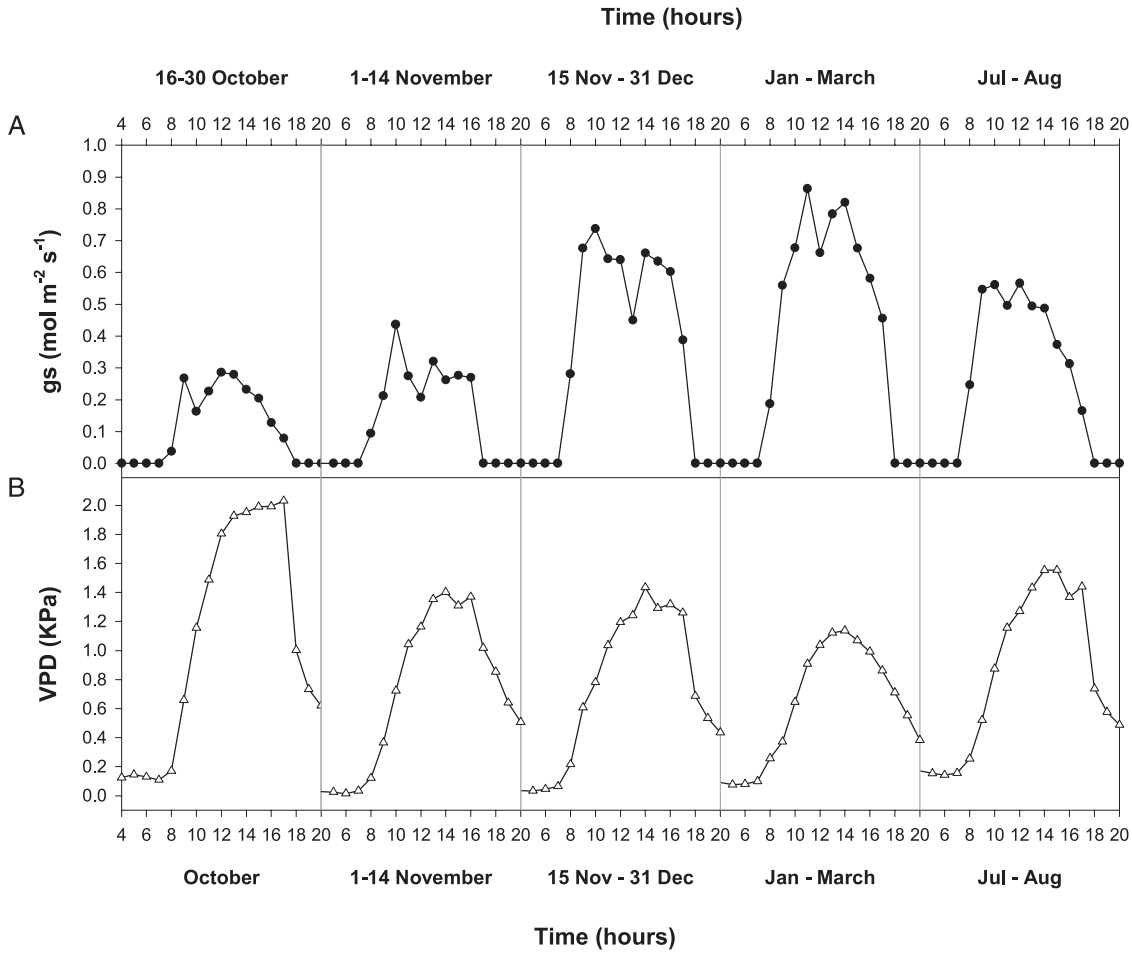

Figure 13. The mean diurnal cycles of canopy conductance, g_s, and atmospheric water vapour pressure deficit, VPD, at various times of the annual cycle. Canopy conductance is poorly defined at night and has been set to zero.

consistently higher in the wet season. On some dry days afternoon values of g_s are lower than morning values but this pattern does not consistently appear on all days. Within the dry season, wet days do not appear to have higher values of g_s than dry days. A possible explanation for this is that the value of g_s is driven by the gradual discharge and recharge of soil moisture reserves, and periods of heavy rain in the dry season only have an effect to the extent that they charge these soil moisture reserves. The forest does not appear to have a direct, rapid response to short (few day) periods of heavy rain. This observation seems to contradict the observation reported above that forest in the early wet season seems to be less stressed than forest in the early dry season at equivalent levels of soil moisture deficit. It is possible that boundary layer feedbacks on VPD may explain this contradiction, with a few days of rain having much less effect on atmospheric VPD, and hence atmospheric water demand, than longer periods of rain.

[61] The annual variations in mean daytime canopy conductance, and in air water vapour deficit, are shown in Figure 12a. The conductances were only calculated for hours with high solar radiation (>400 W m^{-2}) on days without rain. There is a clear correlation between soil moisture status, water vapour deficit and canopy conductance (the former two are shown in Figure 1). Conductance values are at a minimum value of 0.4 mol m^{-2} s^{-1} when flux measurements start in mid-October 1995, a period corresponding to minimum soil water content and high (although not peak) daytime VPDs. Mean conductance then climbs steadily to a value of 0.6 mol m^{-2} s^{-1} by the end of December, as soil moisture content increases, and then fluctuate about this level throughout the wet season, beginning to decline to about 0.5 mol m^{-2} s^{-1} by the early dry season (August 1996).

[62] Atmospheric VPD is correlated with soil moisture status through surface evaporation and planetary boundary layer feedbacks, so it is an interesting question as to whether the annual variation in surface conductance is more driven "from above" by high atmospheric VPDs causing stomatal closure, or "from below" by changes in soil hydraulic conductance, a term that is incorporated in the surface conductance as calculated above. The daytime VPDs are very similar in mid-October 1995 and in August 1996 (Figure 1b). However, g_s is significantly lower in October 1995 than in August 1996, suggesting that it is correlated more directly with soil moisture status, which is significantly lower in October 1995. This finding is corroborated by a modeling sensitivity study of this site by *Williams et al.*

[1998], which suggested that annual variation in soil hydraulic conductance accounted for the majority of the seasonal variation in g_s. Thus, the annual variation in g_s is driven mainly "from below".

[63] Figure 12b explores the relationship with soil moisture further by looking at a select number of days over the year where direct evapotranspiration flux measurements coincided with bi-weekly soil moisture measurements. The relationship between surface conductance and soil moisture content is almost linear (Figure 12c) with a high quality of fit. This provides potentially great predictive value, suggesting that the transpiration of this forest can be predicted directly and simply from soil moisture status.

[64] Figure 12d examines whether the diurnal cycle of g_s is related to variations in VPD, by plotting the mean diurnal cycles of g_s and VPD averaged over the year. There is the expected reduction of g_s with VPD, although it is not clear whether this reduction may be more directly caused by diurnal depletion of soil water reserves close to the root zone.

[65] The mean diurnal cycles of g_s and VPD at various times of year are shown in Figure 13. These show a steady increase in peak values of g_s from 0.3 mol m^{-2} s^{-1} in the dry season to 0.8 mol m^{-2} s^{-1} in the wet season, before decreasing again to 0.5 mol m^{-2} s^{-1} at the start of the following dry season. In the dry seasons there is some indication of a slight asymmetry between morning and afternoon values of g_s, as would be expected if higher afternoon VPDs (Figure 13b) have an effect on stomatal closure.

[66] For comparison, *Shuttleworth* [1989] calculated a peak surface conductance, averaged over three seasons, of 0.5 mol m^{-2} s^{-1} (his results are presented in mm s^{-1}, where 1 mm s^{-1} = 25 mol m^{-2} s^{-1}). For a southern Amazonian rain forest, *Grace et al.* [1995] reported sunny day values of g_s between 0.8 and 1.2 mol m^{-2} s^{-1}.

8. Conclusions

[67] Perhaps the most remarkable feature of the results presented here is that the energy budget of the forest is close to complete closure once transport at low frequencies is taken into account. Non-closure of the energy budget is a feature that has haunted many energy balance studies over forests [e.g., *Aubinet et al.*, 2000], and this finding suggests that solution of the problem, for at least some sites, may lie in consideration of low frequencies. As energy balance closure is one of the few independent tests of the validity of surface flux measurements, the achievement of energy balance closure also greatly increases confidence in the reliability of all flux measurements, at least in the daytime.

[68] If sensible and latent heat fluxes are increased by this reanalysis, it would be expected that fluxes of CO_2 would also be increased by a similar amount, with possible consequences for the estimated net carbon balance. The CO_2 fluxes are indeed found to increase; however, as both daytime and nighttime CO_2 fluxes are increased by a similar amount in opposite directions, the net effect on estimated net carbon balance at this site is negligible (Malhi et al., manuscript in preparation). Hence the inclusion of low frequency turbulent transport does not solve the problem of likely overestimation of net carbon uptake reported for most tropical forest flux sites [*Malhi and Grace*, 2000].

[69] The results presented here show that, while the energy and water dynamics of a fully wetted tropical rain forest are close to expected magnitudes, there are significant seasonal patterns in the energy and water budgets of forests in central Amazonia. As forests in the eastern and southern Amazon tend to have longer dry seasons, seasonal and interannual variations in the intensity of the dry season are likely to influence large areas of Amazonia. These reduction in transpiration are in turn likely to feed back and enhance the dryness of Amazonian climate, as well as affecting the forest carbon and nutrient cycles. While the controlling factors on transpiration rates of fully wetted forest are relatively well measured and easy to describe, a complete description of forest transpiration during dry periods requires understanding of a number of poorly mapped quantities, including plant hydraulic resistances, soil hydraulic properties and root distribution and depth. For this site at least, the total surface conductance is more influenced by soil moisture content than by atmospheric water vapour pressure deficit, and was found to vary linearly with soil water deficit. It is hoped that the data set presented here will provide a useful test for models of forest evapotranspiration and photosynthesis (as shown by *Williams et al.* [1998]). Understanding of the exact spatial pattern of dry season effects will also require description of spatial variations soil hydraulic properties and plant root distribution, both of which are likely to vary significantly over the Amazon Basin. The RAINFOR project (Y. Malhi et al., An international network to understand the biomass and dynamics of Amazonian forests (RAINFLOR), submitted to *Journal Of Vegetation Science*, 2001) is an attempt to measure and understand some of these spatial variations on a basin-wide scale.

[70] The understanding of rain forest response to drought is not only relevant to understanding of the current distribution and function of rain forest. Some climate predictions [e.g., *Cox et al.*, 2000, *White et al.*, 2000] suggest that global climate change will lead to an increased aridification of much of Eastern Amazonia, resulting in the forest being replaced by dry forest, savanna and shrub, with possible major feedbacks on regional and global climate. Understanding the response of tropical forest to drought (both physiologically and ecologically) will be important in predicting their resilience to such possible climatic changes.

[71] **Acknowledgments.** The field work in Brazil was funded through the Terrestrial Initiative on Global Environmental Research (TIGER) of the UK Natural Environment Research Council (NERC), and was part of the Anglo-Brazilian Climate Observation Study (ABRACOS). The field site belongs to the National Institute for Amazonian Research (INPA) in Manaus, Brazil. Y.M. is currently funded by a Royal Society University Research Fellowship, and E.P. is funded by an NERC research grant (GR9/04648).

References

Aubinet, M., et al., Estimates of the annual net carbon and water exchange of forests: The Euroflux methodology, *Adv. Ecol. Res.*, *30*, 113–175, 2000.

Beer, T., *Applied Environmetrics Meteorological Tables*, edited by Appl. Environmetrics, Australia, 1990.

Chauvel, A., M. Grimaldi, and D. Tessier, Changes in soil pore-space

distribution following deforestation and revegetation — An example from the central Amazon Basin, Brazil, *For. Ecol. Manage.*, *38*(3–4), 259–271, 1991.

Choudhury, B. J., N. E. Digirolamo, J. Susskind, W. L. Darnell, S. K. Gupta, and G. Asrar, A biophysical process-based estimate of global land surface evaporation using satellite and ancillary data, II, Regional and global patterns of seasonal and annual variations, *J. Hydrol.*, *205*(3–4), 186–204, 1998.

Correa, J. C., Physical-hydrical characteristics of yellow latosol, red-yellow podzolic, and hydromorphic podzolic soils in the Amazon state, *Pesqui. Agropecu. Bras.*, *19*(3), 347–360, 1984.

Cox, P. M., R. A. Betts, C. D. Jones, S. A. Spall, and I. J. Totterdell, Acceleration of global warming due to carbon-cycle feedbacks in a coupled climate model, *Nature*, *408*(6813), 750, 2000.

Culf, A., G. Fisch, and M. G. Hodnett, The albedo of Amazonian forest and ranch land, *J. Clim.*, *8*(6), 1544–1554, 1995.

Dirmeyer, P. A., and J. Shukla, Albedo as a modulator of climate response to tropical deforestation, *J. Geophys. Res., D: Atmos.*, *99*(D10), 20,863–20,877, 1994.

Eltahir, E. A. B., and R. L. Bras, Precipitation recycling in the Amazon basin, *Q. J. R. Meteorol. Soc.*, *120*(518), 861–880, 1994.

Garratt, J. R., Extreme maximum land surface temperatures, *J. Appl. Meteorol.*, *31*(9), 1096–1105, 1992.

Grace, J., *Plant-Atmosphere Relationships*, 1983.

Grace, J., J. Lloyd, J. Mcintyre, A. Miranda, P. Meir, H. Miranda, J. Moncrieff, J. Massheder, I. Wright, and J. Gash, Fluxes of carbon-dioxide and water-vapor over an undisturbed tropical forest in south-west Amazonia, *Global Change Biol.*, *1*(1), 1–12, 1995.

Henderson-Sellers, A., Continental vegetation as a dynamic component of a global climate model — A preliminary assessment, *Clim. Change*, *23*(4), 337–377, 1993.

Hicks, B. B., and R. T. McMillen, On the measurement of dry deposition using imperfect sensors and in non-ideal terrain, *Boundary-Layer Meteorol.*, *42*, 79–94, 1988.

Hodnett, M. G., L. P. Dasilva, H. R. Darocha, and R. C. Senna, Seasonal soil-water storage changes beneath central Amazonian rain-forest and pasture, *J. Hydrol.*, *170*(1–4), 233–254, 1995.

Laurance, W. F., M. A. Cochrane, S. Bergen, P. M. Fearnside, P. Delamonica, C. Barber, S. D'angelo, and T. Fernandes, Environment — The future of the Brazilian Amazon, *Science*, *291*(5503), 438–439, 2001.

Leopoldo, P. R., W. K. Franken, and N. A. V. Nova, Real evapotranspiration and transpiration through a tropical rain-forest in central Amazonia as estimated by the water- balance method, *For. Ecol. Manage.*, *73*(1–3), 185–195, 1995.

Luizão, F. J., and H. O. R. Shubert, Litter production and mineral element input to the forest floor in a central Amazonian forest, *GeoJournal*, *19*, 407–417, 1989.

Malhi, Y., and J. Grace, Tropical forests and atmospheric carbon dioxide, *Trends Ecol. Evol.*, *15*(8), 332–337, 2000.

Malhi, Y., A. D. Nobre, J. Grace, B. Kruijt, M. G. P. Pereira, A. Culf, and S. Scott, Carbon Dioxide Transfer Over A Central Amazonian Rain Forest, *Journal Of Geophysical Research-Atmospheres*, *103*(D24), 31,593–31,612, 1998.

Moncrieff, J., R. Valentini, S. Greco, G. Seufert, and P. Ciccioli, Trace gas exchange over terrestrial ecosystems: Methods and perspectives in micrometeorology, *J. Exp. Bot.*, *48*(310), 1133–1142, 1997.

Monteith, J. L., and M. H. Unsworth, *Principles Of Environmental Physics*, 1990.

Moore, C. J., Frequency-response corrections for eddy-correlation systems, *Boundary Layer Meteorol.*, *37*(1–2), 17–35, 1986.

Moore, C. J., and G. Fisch, Estimating heat-storage in Amazonian tropical forest, *Agric. For. Meteorol.*, *38*(1–3), 147–168, 1986.

Nepstad, D. C., C. R. Decarvalho, E. A. Davidson, P. H. Jipp, P. A. Lefebvre, G. H. Negreiros, E. D. Dasilva, T. A. Stone, S. E. Trumbore, and S. Vieira, The role of deep roots in the hydrological and carbon cycles of Amazonian forests and pastures, *Nature*, *372*(6507), 666–669, 1994.

Nobre, C. A., P. J. Sellers, and J. Shukla, Amazonian deforestation and regional climate change, *J. Clim.*, *4*(10), 957–988, 1991.

Paulson, C. A., The mathematical representation of wind speed and temperature profiles in the unstable surface layer, *J. Appl. Meteorol.*, *9*, 857–861, 1970.

Ribeiro, M. D. G., and J. Adis, Local rainfall variability — A potential bias for bioecological studies in the central Amazon, *Acta Amazonica*, *14*, 159–174, 1984.

Roberts, J., O. M. R. Cabral, G. Fisch, L. C. B. Molion, C. J. Moore, and W. J. Shuttleworth, Transpiration from an Amazonian rain-forest calculated from stomatal conductance measurements, *Agric. For. Meteor.*, *65*(3–4), 175–196, 1993.

Shuttleworth, W. J., Micrometeorology of temperate and tropical forest, *Philos. Trans. R. Soc. London, Ser. B*, *324*(1223), 299–334, 1989.

Shuttleworth, W. J., et al., Eddy-correlation measurements of energy partition for Amazonian forest, *Q. J. R. Meteorol. Soc.*, *110*(466), 1143–1162, 1984.

Trenberth, K. E., Atmospheric moisture recycling: Role of advection and local evaporation, *J. Clim.*, *12*(5), 1368–1381, 1999.

White, A., M. G. R. Cannell, and A. D. Friend, CO_2 stabilization, climate change and the terrestrial carbon sink, *Global Change Biol.*, *6*(7), 817–833, 2000.

Williams, M., Y. Malhi, A. D. Nobre, E. B. Rastetter, J. Grace, and M. G. P. Pereira, Seasonal variation in net carbon exchange and evapotranspiration in a Brazilian rain forest: A modelling analysis, *Plant Cell Environ.*, *21*(10), 953–968, 1998.

Xue, Y. K., H. G. Bastable, P. A. Dirmeyer, and P. J. Sellers, Sensitivity of simulated surface fluxes to changes in land surface parameterizations — A study using Abracos data, *J. Appl. Meteorol.*, *35*(3), 386–400, 1996.

R. Clement, J. Grace, Y. Malhi, and E. Pegoraro, Institute of Ecology and Resource Management, University of Edinburgh, Darwin Building, Mayfield Road, Edinburgh EH9 3JU, Scotland, UK.

A. D. Nobre, Instituto Nacional de Pesquisas da Amazônia, Manaus, Amazonas, Brazil.

M. G. P. Pereira, Universidade Federal de Viçosa, Minas Gerais, Brazil.

A. D. Culf, Centre for Ecology and Hydrology, Wallingford, UK.